

High- T_C surface superconductivity in topological Weyl semimetal t-PtBi₂

Sebastian Schimmel^{1,2}, Yanina Fasano^{2,3}, Sven Hoffmann^{1,2}, Joaquín Puig^{2,3}, Grigory Shipunov^{2,*}, Danny Baumann², Saicharan Aswartham², Bernd Büchner^{2,4}, Christian Hess^{1,2}

¹ *Fakultät für Mathematik und Naturwissenschaften, Bergische Universität Wuppertal, 42097 Wuppertal, Germany*

² *Leibniz-Institute for Solid State and Materials Research (IFW-Dresden), Helmholtzstraße 20, 01069 Dresden, Germany*

³ *Instituto de Nanociencia y Nanotecnología and Instituto Balseiro, CNEA – CONICET and Universidad Nacional de Cuyo, Centro Atómico Bariloche, Avenida Bustillo 9500, 8400 Bariloche, Argentina*

⁴ *Institute of Solid State and Materials Physics and Würzburg-Dresden Cluster of Excellence ct.qmat, Technische Universität Dresden, 01062 Dresden, Germany*

**Present address: Institute of Physics, University of Amsterdam, 1098 XH Amsterdam, The Netherlands*

Summary

Topological superconductivity is a very promising concept for generating fault tolerant qubits in quantum computation¹⁻³. Early experimental achievements study hybrid systems⁴⁻⁵ as well as doped intrinsic topological or superconducting materials⁶⁻⁸. These pioneering results concern either inconclusive phenomenology or very-low temperatures. In a very recent work intrinsic two-dimensional low-temperature superconductivity has been reported in the type-I Weyl semimetal trigonal PtBi₂⁹. However, larger critical temperatures are indispensable for technological exploitation. Here we show that trigonal PtBi₂ possesses high-temperature surface superconductivity. By means of scanning

tunnelling spectroscopy we reveal that the superconducting gap can be as large as 20 meV, suggesting a critical temperature in the 100 K range, like in cuprate high-temperature superconductors. To our knowledge, this is the largest superconducting gap that has been observed so far in a topological material. The superconducting state at 5 K persists up to Tesla-range applied fields and the upper critical field at this temperature is of roughly 12 Tesla. Our results therefore render trigonal PtBi₂ a prime candidate for topological superconductivity at technologically relevant temperatures.

The quest for materials presenting an interplay between superconductivity and topologically protected electronic surface states has sped up recently due to their exciting possibilities of application in emergent quantum technologies^{2-3, 10-18}. For instance, Majorana fermions are promising candidates for realizing quantum computation topologically protected from decoherence¹. These zero energy modes can be hosted by ferromagnetic atomic chains on a superconductor^{1,4-5}, topological quantum spin liquids¹⁹⁻²¹, and topological materials with superconducting properties²²⁻²⁶. Among the latter, semimetals with linear dispersing bands have recently attracted the attention of the materials science community²⁷⁻²⁸. In particular, there have been reports on the interplay of superconductivity and type II Weyl semimetal behavior in transition metal dichalcogenides^{13,16}. In Weyl semimetals strong spin-orbit coupling and broken time reversal or inversion symmetry lift the degeneracy of the linear dispersive bands, a condition that might allow the establishment of topological superconductivity^{12,23}.

Despite the great interest of the scientific community on this subject, only one month ago it was disclosed that the electronic structure of the van der Waals layered trigonal PtBi₂ (t-PtBi₂) renders it a type-I Weyl semimetal⁹. Transport measurements on bulk crystals earlier revealed superconductivity with a critical temperature of up to 0.6 K (ref. ²⁹), and a Berezinskii-Kosterlitz-Thouless transition in flakes with thickness up to tens of nanometers, providing support for two-dimensional superconductivity, has been reported very recently⁹.

Motivated by these interesting findings, here we report on low-temperature scanning tunnelling microscopy (STM) and spectroscopy data in t-PtBi₂ at 5 down to 30 mK and high magnetic fields. The low-temperature tunnelling differential conductance dI/dV_B is directly proportional to the local density of states (LDOS). Thus our data provide direct access to the LDOS at the surface with atomic resolution³⁰. In particular, this technique can probe the surface of t-PtBi₂ for a superconducting LDOS and quantify the magnitude of its energy gap. Moreover, it can provide a one-to-one relation between superconducting and topographic properties.

Results

Our topographic STM measurements on t-PtBi₂ (Fig. 1) reveal two types of cleaved surfaces, in agreement with a previous report³¹. In this earlier work no signatures of superconductivity were reported. As is shown in the schematics of the crystal structure of Fig. 1, t-PtBi₂ is composed of layers stacked along the **c**-axis where coplanar Pt atoms are sandwiched in between two sheets of Bi atoms. In one sheet the Bi atoms are coplanar too,

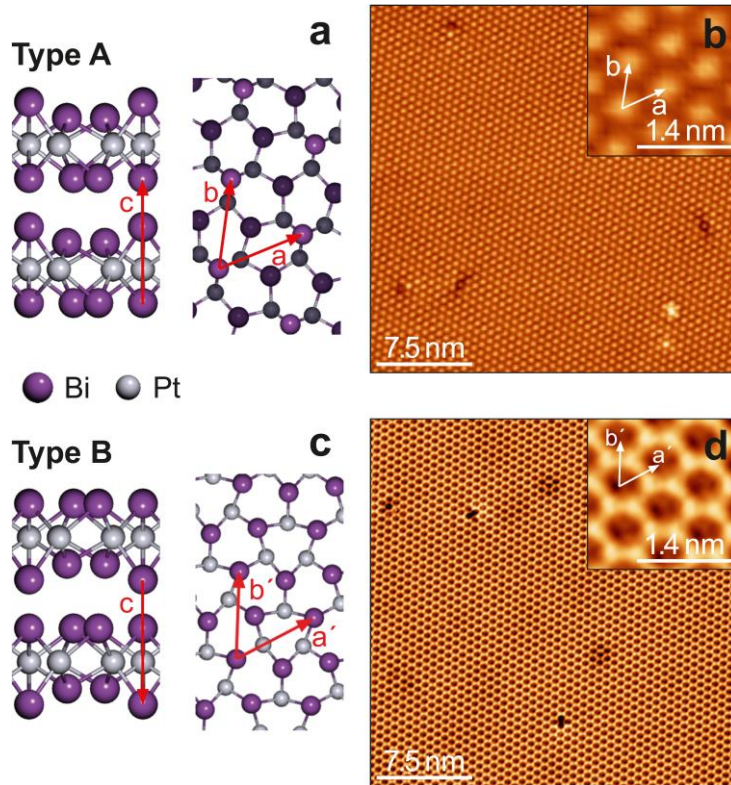


Figure 1: Crystal structure and STM topographies of non-centrosymmetric trigonal PtBi_2 . (a) Schematics of the crystal structure with the sample terminating at a corrugated Bi plane (type A surface). Left: lateral view with the lattice parameter $c = 6.167 \text{ \AA}$ (ref. ²⁹) indicated. Right: Top view with the in-plane lattice parameters indicated, $a = b = 6.573 \text{ \AA}$ (ref. ²⁹). The topmost Bi atoms of the last layer are shown brighter. (b) Constant current topographic image of the typical atomic corrugation of a type A surface with bright spots arranged in a hexagonal lattice ($29 \times 29 \text{ nm}^2$, 400 pA and 350 mV). (c) Crystal structure in which the surface Bi atoms are in a coplanar arrangement (type B surface). Left: lateral view. Right: Top view with the in-plane lattice parameters indicated. (d) Constant current topographic image of the typical atomic corrugation observed on type B surface resembling a honeycomb structure ($29 \times 29 \text{ nm}^2$, 800 pA and 7.5 mV). Inserts: Zoom-ins of the main images with the unit cell vectors indicated. All measurements performed at $T = 30 \text{ mK}$.

but the other has a corrugation on the location of Bi atoms in the c-axis direction. These two types of Bi sheets are pairwise van der Waals bonded, and the natural cleaving plane is thus in between these layers. We label the two different corrugated and flat Bi cleaved surfaces as type A and B, respectively.

Figure 2 shows the most important result of this work: The surfaces of t-PtBi₂ present a superconducting quasiparticle excitation spectrum even at a surprisingly high temperature of 5 K, one order of magnitude larger than the previously reported transport $T_c \approx 0.6$ K (ref. ⁹). The STM spectra exhibit a depletion close to zero bias and particle-hole symmetric coherence peaks at low applied magnetic fields. This can be well recognized in Fig. 2 (a) which shows zero magnetic field data of the dI/dV_B measured on a type B surface at $T = 5$ K. Fitting the data with an s-wave BCS density of states plus a Dynes term accounting for the quasiparticles' lifetime shortening estimates a superconducting gap of $\Delta = 10.1 \pm 0.1$ meV. A further inspection on this particular surface over several weeks revealed robust superconductivity, even for relatively large applied magnetic fields. Figure 2 (b) shows a dI/dV_B spectrum measured at $B = 9$ T on the same cleaved surface. Remarkably, the BCS fit yields an even larger superconducting gap $\Delta = 20.3 \pm 0.2$ meV. Note that the observed Δ values suggest high- T_c superconductivity of the here investigated surfaces of t-PtBi₂. A simple rule of thumb calculation using the BCS ratio in the weak coupling case, $2\Delta/k_B T_c = 3.5$, yields an astonishingly high critical temperature of roughly 65 and 130 K for the data in Fig. 2 (a) and (b), respectively. These values are comparable to those found in cuprate high- T_c superconductors³⁰.

Figure 2 (c) shows a systematic investigation of the superconducting LDOS as a function of field up to $B = 15$ T. Up to 9 T no significant effect of the magnetic field is observable but upon increasing B to 12 T the coherence peaks fade away and the depletion in the low-energy conductance fills in, indicative of $B_{c2} \approx 12$ T.

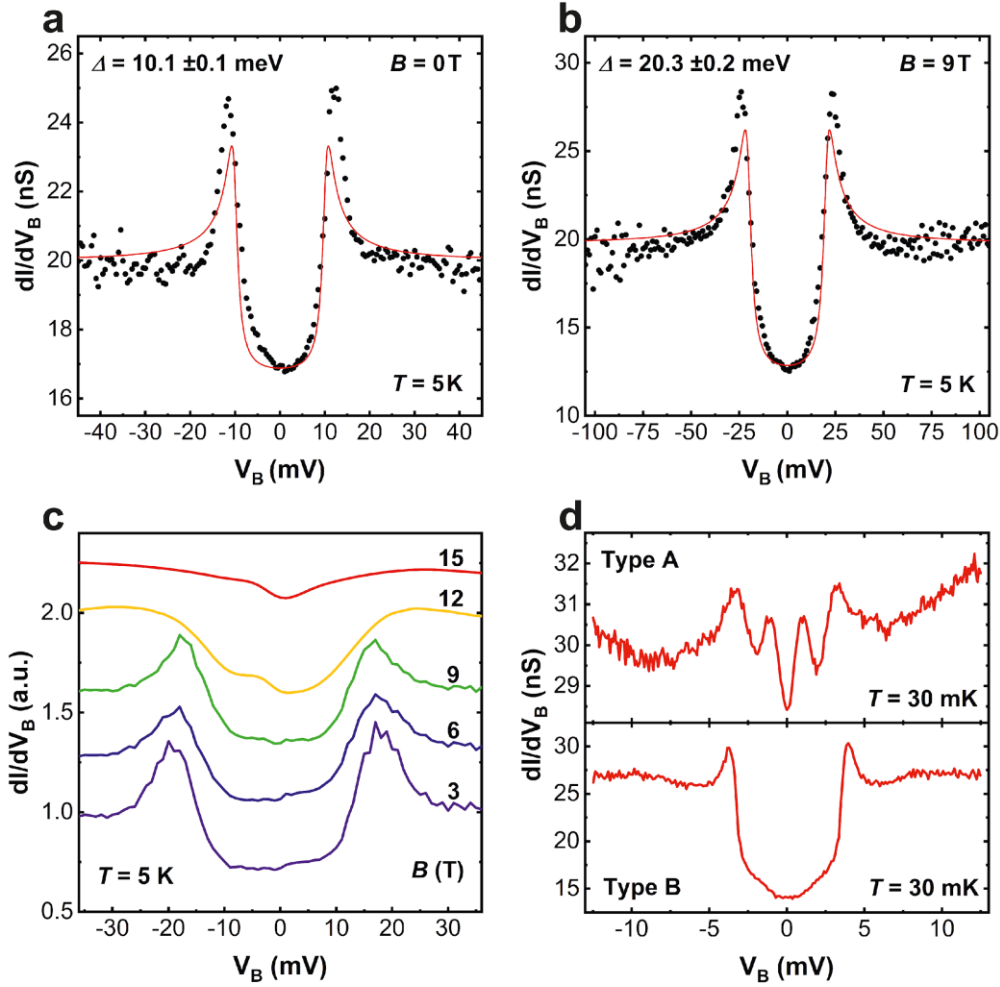


Figure 2: Superconducting gap of t-PtBi₂ and its closing with field. (a) Example of a dI/dV_B spectrum (black circles) measured at zero field in a type B surface (stabilisation conditions $V_B = 50\text{ mV}$, $I = 1\text{ nA}$). The red line is a fit to the data considering an s -wave BCS density of states with a Dynes quasiparticle lifetime shortening term yielding a gap of $\Delta = 10.1 \pm 0.1\text{ meV}$. (b) STM spectrum measured at $B = 9\text{ T}$ in a particular region of the same sample where we observed the maximum superconducting gap of $\Delta = 20.3 \pm 0.2\text{ meV}$ (stabilisation conditions: $V_B = 150\text{ mV}$, $I = 3\text{ nA}$). (c) Evolution of the quasiparticle excitation spectrum (normalized tunnel conductance) with the applied field, acquired in the same cleaved surface (stabilisation conditions: $B = 3, 9, 12, 15\text{ T}$, $V_B = 150\text{ mV}$, $I = 3\text{ nA}$; $B = 6\text{ T}$, $V_B = 100\text{ mV}$, $I = 2\text{ nA}$). (d) dI/dV spectra measured on two samples of opposite surface type exhibiting a smaller superconducting gap (stabilisation conditions: $V_B = 25$ (15) mV, $I = 0.8$ (0.4) nA, $V_{\text{mod}} = 200$ (150) μV , $f_{\text{mod}} = 667$ (667) Hz for type A (type B) surface).

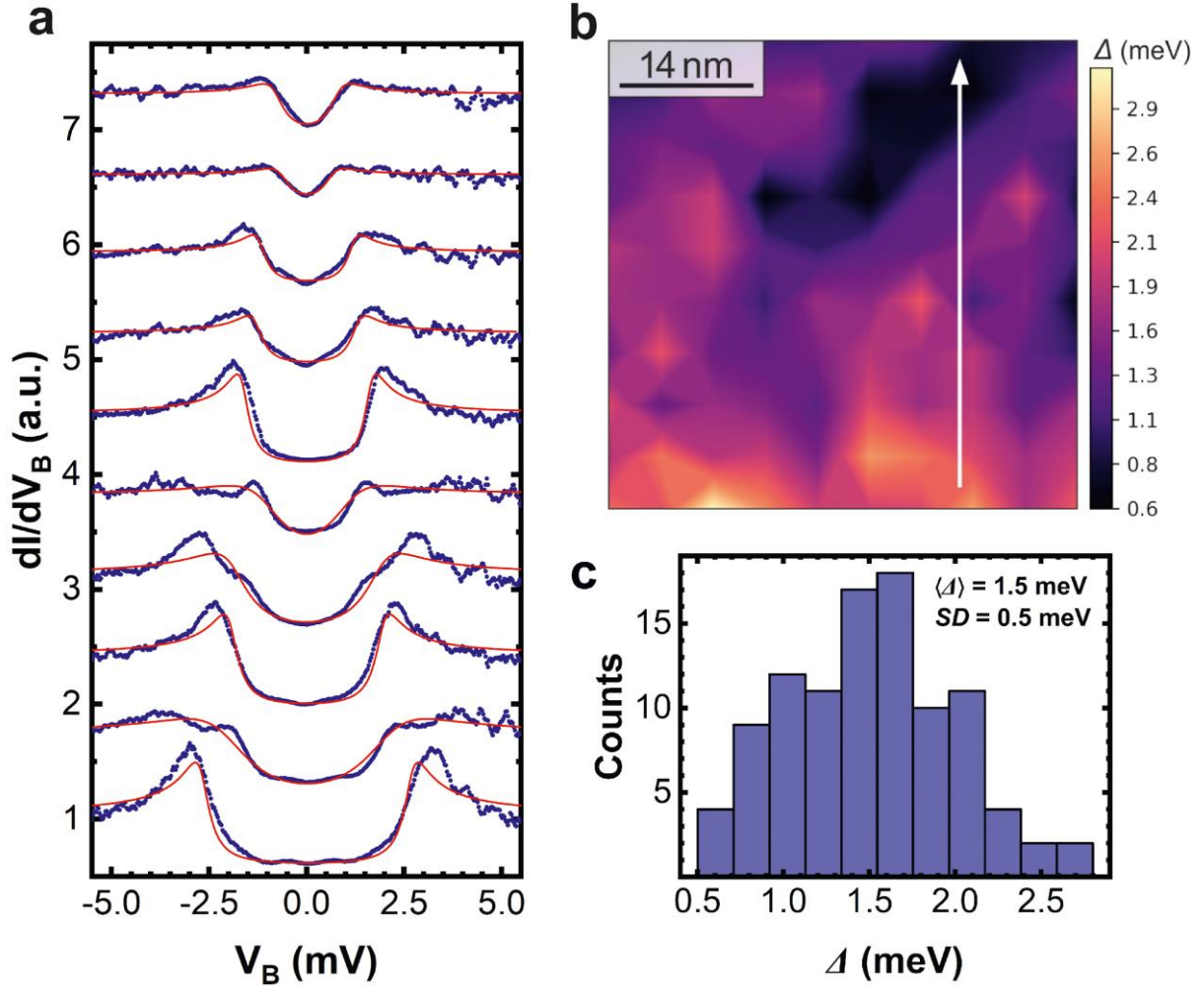


Figure 3: Spatial inhomogeneity of the superconducting gap for a type B atomically flat terrace of t-PtBi₂ measured at zero field. (a) Trace of ten normalized dI/dV_B curves out of a 10 x 10 grid covering an area of 50 x 50 nm². The experimental data are shown with blue circles whereas red lines correspond to fits to the data with an s-wave BCS density of states considering a Dynes quasiparticles' lifetime shortening term. (b) Map of the local value of the superconducting gap obtained from the fits. The vertical white arrow indicates the location where the trace of spectra of panel (a) was acquired. (c) Histogram of the superconducting gap values shown in (b) indicating the mean $\langle \Delta \rangle$ and geometrical standard deviation SD values. The measurements were performed at 30 mK in sample #10 with regulation conditions 1.5 nA and 15 mV.

Having established the spectral features of superconducting surfaces of t-PtBi₂ we now turn to the variability of the superconducting gap. This variability is apparently significant since the value of Δ found for the spectra in Fig. 2 (a) and (b) differs roughly by a factor of 2 implying that superconductivity is not spatially homogenous even if measured on the same surface.

Interestingly, further experiments on different surfaces of t-PtBi₂ yield a large variability of the gap ranging from complete absence of superconductivity over relatively small $\Delta = 1-3$ meV to the just discussed very large $\Delta = 10-20$ meV, see Extended Data Fig. 1. Note that signatures of superconductivity are observed on both types of surfaces, see Fig. 2 (d).

In order to further support the intrinsic nature of the spatially varying superconducting gap even at very local scale, we show in Fig. 3 (b) a gap map of the type B surface of sample #10 covering a 50×50 nm² field of view. In this nanoscale area the values of the gap ranging from 0.5 to 3 meV clearly demonstrate the large variability of Δ and provide clear-cut evidence of its spatial inhomogeneity.

Discussion

The observed superconductivity is remarkably robust: In all cases where a finite superconducting gap is observed, the BCS ratio implies large values for T_c which are 1-2 orders of magnitude larger than those reported in transport measurements (ref. ^{9,29}). Experimentally, there is a strong difference between the transport and STM/STS data with respect to probing the superconducting state. While the former probes the bulk of the investigated samples, STM primarily probes the surface superconductivity. Note that there is no match between transport $T_c = 0.6$ K and the here measured gap sizes observed at $T = 5$ K. In order to reconcile this discrepancy, one might speculate that the transport T_c marks the transition from surface to bulk superconductivity, at least for tens of nanometre-thick flakes⁹.

In fact, the notion of surface superconductivity at 5 K being probed by STM is corroborated by the relatively low depletion of the LDOS at zero bias voltage of only roughly 25-50% observed in most of the spectra. This is very well compatible with the LDOS of a surface superconductor superimposed to the bulk LDOS of a normal metal.

Now, since t-PtBi₂ is predicted to be a type I Weyl semimetal hosting topologically non-trivial surface states⁹, the straightforward question is whether the superconductivity of this

material is connected to the surface states. If this were the case, our data would constitute the first direct observation of superconductivity emerging from the topological surface states of a type I Weyl semimetal.

In a first step into further characterising the surface superconducting state, the magnetic field data can be exploited. In particular, the closing of the gap at around 12 T can be taken as a rough estimate of the orbital limiting field $B_{c2} = \Phi_0/2\pi\xi^2$. Remarkably, the resulting coherence length $\xi \approx 5$ nm is extremely short, similar to what is known for high- T_c superconductors³⁰ and, more importantly, it is 1-2 orders of magnitude smaller than that measured in transport.

While our main conclusion of surface superconductivity in t-PtBi2 is very robust, there are some caveats requiring further experimental work beyond the scope of this paper. On one hand, our data do not disprove that topologically trivial surface or bulk states play a role for forming the superconducting state. Future work is required to directly reveal whether the gapped density of states is connected to the topological surface states. On the other hand, despite all our efforts, we were not able to image vortices (see Extended Data Fig. 2). At present, we do not have a clear explanation but we conjecture that a creeping flux lattice prevented us from vortex detection.

Finally, another puzzling finding is the large variability of the gap size on different surfaces. One possible reason could be found in the van der Waals coupling of the t-PtBi2 layers and the resulting tendency to exfoliate. In fact, upon cleaving the samples we frequently observed unstable cantilevered flakes on which STM measurements could not be performed as well as stable surfaces where some areas of the topographies reveal a proliferation of wrinkles and foldings at the top layer. While our data have typically been registered on hundreds of nanometre-sized atomically flat terraces, one should consider the possibility that the observed variability of superconductivity could be connected with variations of the coupling of the topmost layers and the underlying bulk.

In conclusion, we provide strong evidence of high temperature superconductivity on the surface of t-PtBi₂ with gaps reaching the surprisingly large value of 20 meV, roughly corresponding to $T_c = 130$ K. The superconductivity is robust against out of plane fields up to about 12 T and also exhibits a significant variability within a surface and even stronger from one prepared surface to another, resembling the phenomenology of underdoped cuprates. This qualifies t-PtBi₂ as a novel platform to achieve high-temperature superconductivity.

Moreover, since this material is predicted to be a type I Weyl semimetal with topological surface states, our data might reflect the first example of superconductivity emerging from topological Weyl surface electrons. Indeed, an intrinsic topological high-temperature superconductor is of fundamental importance since it may offer a new route to engineer Majorana surface modes stable at temperatures which are easily reachable by nitrogen-cooling.

References

1. Kitaev, A. Yu. Unpaired Majorana fermions in quantum wires. *Phys.-Usp.* **44** 131 (2001)
2. Alicea, J. New directions in the pursuit of Majorana fermions in solid state systems. *Rep. Prog. Phys.* **75**, 076501 (2012).
3. Beenaker, C. W. J. Search for Majorana fermions in Superconductors. *Annu. Rev. Condens. Matter Phys.* **4**, 113 (2013)
4. Nadj-Perge, S. *et al.* Observation of Majorana fermions in ferromagnetic atomic chains on a superconductor. *Science* **346**, 6209 (2014).
5. Crawford, D. *et al.* Majorana modes with side features in magnet-superconductor hybrid systems. *npj Quantum materials* **7**, 117 (2022).
6. Sato, M. & Ando, Y. Topological superconductors: a review. *Rep. Prog. Phys.* **80**, 076501 (2017)

7. Wang, D. *et al.* Evidence for Majorana bound states in an iron-based superconductor. *Science* **362**, 333 (2018)
8. Machida, T. *et al.* Zero-energy vortex bound state in the superconducting topological surface state of Fe(Se,Te). *Nat. Mater.* **18**, 811 (2019).
9. Veyrat, A. *et al.* Berezinskii-Kosterlitz-Thoules Transition in the Type-I Weyl Semimetal PtBi₂. *ACS Nano Lett.* <https://doi.org/10.1021/acs.nanolett.2c04297>
10. Cho, G. Y., Bardarson, J. H., Lu, Y.-M., & Moore, J. E. Superconductivity of doped Weyl semimetals: Finite-momentum pairing and electronic analog of the ³He-A phase. *Phys. Rev. B* **86**, 214514 (2012).
11. Wei, H., Chao, S. -P., & Aji, V. Odd-parity superconductivity in Weyl semimetals. *Phys. Rev. B* **89**, 014506 (2014).
12. Hosur, P., Dai, X., Fang, Z., & Qi, X. -L. Time-reversal-invariant topological superconductivity in doped Weyl semimetals. *Phys. Rev. B* **90**, 045130 (2014).
13. Qi, Y. *et al.* Superconductivity in Weyl semimetal candidate MoTe₂. *Nature Comm.* **7**, 11038 (2016).
14. Bachmann, M. *et al.* Inducing superconductivity in Weyl semimetal microstructures by selective ion sputtering. *Sci. Adv.* **3**, e1602983 (2017).
15. Huang, C. *et al.* Inducing Strong Superconductivity in WTe₂ by a Proximity Effect. *ACS Nano* **12**, 7185 (2018).
16. Naidyuk, Y. *et al.* Surface superconductivity in the Weyl semimetal MoTe₂ detected by point contact spectroscopy. *2D Mater.* **5** 045014 (2023).
17. Huang, C. *et al.* Proximity-induced surface superconductivity in Dirac semimetal Cd₃As₂. *Nat. Comm.* **10**, 2217 (2019).
18. Dong W. -H. *et al.* Superconductivity and topological aspects of two-dimensional transition-metal monohalides. *npj Comput. Mater.* **8**, 185 (2022).
19. Kitaev, A. Anyons in an exactly solved model and beyond. *A. Ann. Phys.* **321**, 2 (2006).

20. Kasahara, Y. *et al.* Majorana quantization and half-integer thermal quantum Hall effect in a Kitaev spin liquid. *Nature* **559**, 227 (2018)
21. Wolter, A. U. B. & Hess, C. Spin liquid evidence at the edge and in bulk. *Nat. Phys.* **18**, 370 (2022).
22. Fu, L. & Kane, C. L. Superconducting Proximity Effect and Majorana Fermions at the Surface of a Topological Insulator. *Phys. Rev. Lett.* **100**, 096407 (2008).
23. Meng, T. & Balents, L. Weyl superconductors. *Phys. Rev. B* **86**, 54504 (2012).
24. Li, Y & Haldane, F. D. M. Topological Nodal Cooper Pairing in Doped Weyl Metals, *Phys. Rev. Lett.* **120**, 067003 (2018).
25. Yuan, Y. *et al.* Evidence of anisotropic Majorana bound states in 2M-WS₂. *Nat. Phys.* **15**, 1046 (2019).
26. Yan, Z., Wu, Z., & Huang, W. Vortex End Majorana Zero Modes in Superconducting Dirac and Weyl Semimetals. *Phys Rev Lett.* **124**, 257001 (2020).
27. Kopnin, N. B., Heikkilä, T. T., & Volovik, G. E. High-temperature surface superconductivity in topological flat-band systems. *Phys. Rev. B* **83**, 220503 (2011).
28. Sharma, M. M., Sharma, P., Karn, N. K., & Awana, V. P. S. Comprehensive review on topological superconducting materials and interfaces. *Supercond. Sci. Technol.* **35**, 083003 (2022).
29. Shipunov, G. *et al.* Polymorphic PtBi₂: Growth, structure, and superconducting properties. *Phys. Rev. Materials* **4**, 124202 (2020).
30. Fischer, Ø., Kugler, M., Maggio-Aprile, I., Berthod, Ch., & Renner, Ch. Scanning tunneling spectroscopy of high-temperature superconductors. *Rev. Mod. Phys.* **79**, 353 (2007).
31. Nie, X. -A. *et al.* Robust Hot Electron and Multipole Topological Insulator States in PtBi₂. *ACS Nano* **14**, 2366 (2020).

Methods

Crystal growth and characterisation

We studied ten samples of single crystalline t-PtBi₂ grown by means of the self-flux method as described in Ref. ²⁹. The composition and crystal structure of the samples were determined by energy-dispersive x-ray spectroscopy and x-ray diffraction, respectively. In-plane resistivity was measured applying the four probe method as a function of temperature in the ranges 0.1 – 300 K using ⁴He and dilution cryostats. Evidence of superconductivity has been found below 600 mK (ref. ²⁹).

STM setups

The measurements were carried out in two home-build low-temperature scanning tunnelling microscope setups with Nanonis SPM control systems³³. Mechanically sharpened PtIr tips served as the ground electrode. Data measured at $T = 5$ K was acquired by a liquid-helium-cooled scanning tunneling microscope with an energy resolution of ≈ 2 meV (ref. ³²). Equipped with a superconducting magnet, this system allows us to execute field-dependent studies up to $B = 15$ T. We also used a second setup where the STM is attached to a dilution refrigerator yielding measurement temperatures down to 30 mK. This system has an improved energy resolution in the sub-meV regime. In order to prepare pristine atomically clean surfaces prior to the measurements, the platelet-like samples were cleaved in both devices at $T \sim 5$ K in cryogenic ultra-high vacuum atmosphere.

Data acquisition and processing

Standard STM measurement techniques like the constant current and the $I(V_B)$ spectroscopy modes were applied to acquire the topographic and spectroscopic data, respectively. The dI/dV_B spectra were obtained by numerical differentiation of the $I(V_B)$ curves or via the commonly used lock-in technique - if used, indicated by the modulation parameters

V_{mod} and f_{mod} . The data were analysed using the software for scanning probe microscopy WSxM³⁴.

In addition, in order to estimate the value of the superconducting gap we wrote a fitting program in Python language. The spectra were fitted using an s-wave BCS density of states, the Dynes parameter Γ (ref. ³⁵), and an additional constant D accounting for the contribution of a non-superconducting background:

$$dI/dV_B(V_B) = C |\text{Re}\{(eV_B - i\Gamma)/[(eV_B - i\Gamma)^2 - \Delta^2]^{1/2}\}| + D$$

In the formula C is a proportionality constant, e denotes the charge of an electron and Δ is the superconducting gap. The broadening of spectroscopic features due to a finite quasiparticle lifetime is taken into account by the phenomenological Dynes parameter Γ .

Measurements in magnetic field

The magnetic field dependence of the superconducting state was systematically studied after a zero-field cooling process: The samples were cooled down to ~ 5 K and then the field was applied. We measured increasing the field in steps $B = 3, 6, 9$ T, and then the field was set to the maximum available field of 15 T at which the superconducting gap was suppressed. Afterwards, the field was reduced to 12 T at which the superconducting gap was observed in the spectrum again. In order to guarantee the comparability of the spectra, throughout these investigations the tunnelling junction stabilisation resistance was kept constant at 50 M Ω .

Data availability

The data supporting the findings of this study are available from the corresponding author upon reasonable request. Source data are provided with this paper.

32. Schlegel, R. *Et al.* Design and properties of a cryogenic dip-stick scanning tunneling microscope with capacitive coarse approach control. *Rev. Sci. Instrum.* **85**, 013706 (2014).
33. SPECS Surface Nano Analysis GmbH, Voltastrasse 5 13355 Berlin / Germany, webpage: <https://www.specs-group.com/nanonis/products/> (2016).
34. Horcas, I. *et al.* WSXM: A software for scanning probe microscopy and a tool for nanotechnology. *Rev. Sci. Instrum.* **78**, 013705 (2007).
35. Dynes, R. C., Narayanamurti, V., Garno, J.P. Direct Measurement of Quasiparticle-Lifetime Broadening in a Strong-Coupled Superconductor *Phys. Rev. Lett.* **41**, 1509 (2007).

Acknowledgements

Work supported by the European Research Council (ERC) under the European Union's Horizon 2020 research and innovation programme (Grant Agreement No. 647276-MARS-ERC-2014-CoG) and by the Deutsche Forschungsgemeinschaft (DFG, German Research Foundation) Grants 500507880 and AS 523/4-1. Y.F. acknowledges support from the Georg Forster Research Prize from the Alexander von Humboldt Foundation.

Author Contributions

C. H, S. S., and B. B. designed the research, S. S., S. H., J. P., Y.F., and D.B. performed measurements, G. S. and S.A. grew samples, S. S., S. H., J. P., and Y.F. analysed data; all authors discussed the data analysis and interpretation; S. S., Y.F., J. P., and C. H. wrote the paper.

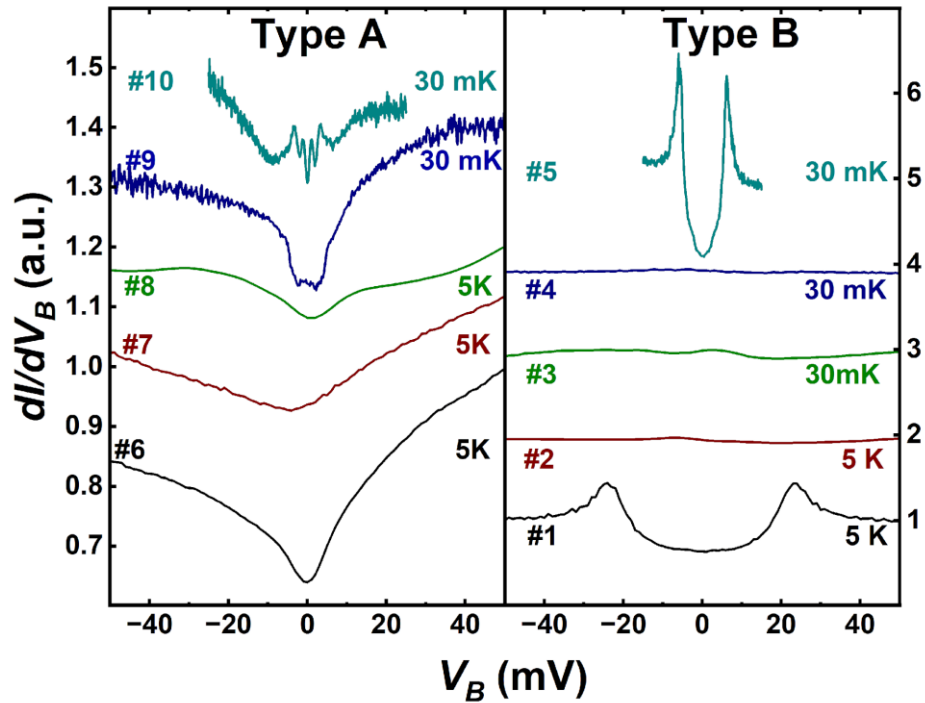
Competing interests

The authors declare no competing interests.

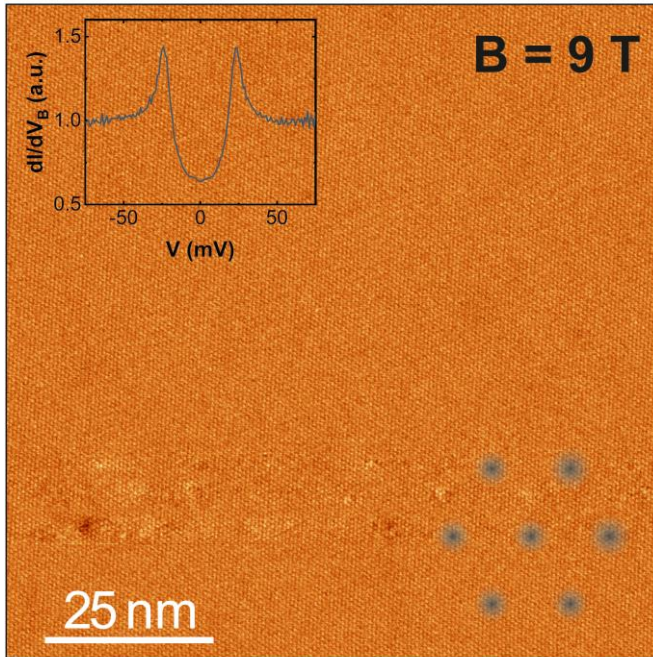
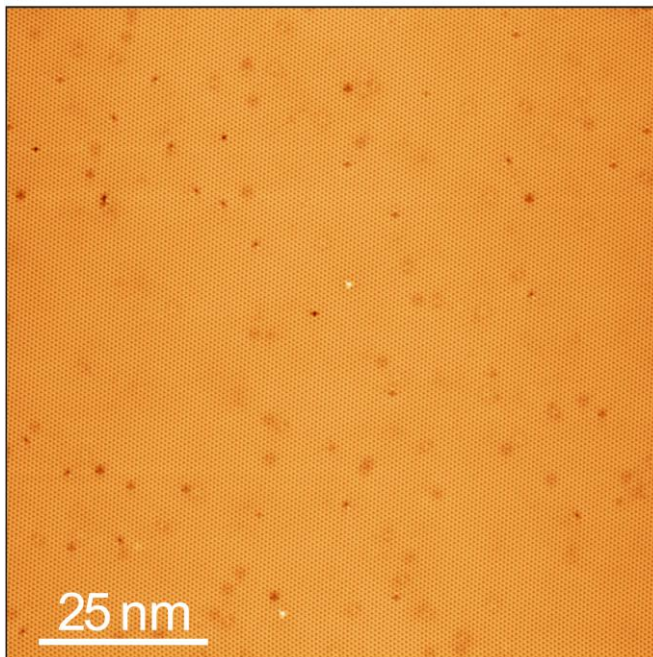
Corresponding author

Correspondence to Sebastian Schimmel and Christian Hess

Extended data



Extended Data Figure 1: Typical normalized tunnel conductance spectra measured in the 10 t-PtBi₂ samples studied. Left panel: Data in type A surface. Right panel: Data in type B surfaces. Spectra have been shifted vertically for clarity. Measurements performed at 5 and 0.03 K.

a**b**

Extended Data Figure 2: (a) Typical zero bias conductance map measured at 9 T and 5 K in the type B surface of t-PtBi₂ sample #1. No signatures of local variations of conductance as expected when nucleating three dimensional vortices are observed even though the map registers the atomic corrugation. Top left insert: Typical tunnel conductance spectra acquired in the region where the zero bias conductance map was measured. Bottom right insert: Schematics of the three dimensional vortex structure expected for 9T with a lattice spacing of 16 nm. (b) Simultaneously acquired atomic-resolution topography of the region measured in panel (a). Stabilisation conditions were 100 pA and 1.2 mV.